Structural and elastic properties of a confined two-dimensional colloidal solid: A molecular dynamics study

M. Ebrahim Foulaadvand[1,2,*] and Neda Ojaghlou[1]

[1]*Department of Physics, Zanjan University, P.O. Box 19839-313, Zanjan, Iran*

[2]*Computational Physical Sciences Laboratory, Department of Nano-Science, Institute for Research in Fundamental Sciences (IPM), P.O. Box 19395-5531, Tehran, Iran*

(Received 11 February 2012; revised manuscript received 30 July 2012; published 23 August 2012)

We implement molecular dynamics simulations in canonical ensemble to study the effect of confinement on a two-dimensional crystal of point particles interacting with an inverse power law potential proportional to r^{-12} in a narrow channel. This system can describe colloidal particles at the air-water interface. It is shown that the system characteristics depend sensitively on the boundary conditions at the two *walls* providing the confinement. The walls exert perpendicular forces on their adjacent particles. The potential between walls and particles varies as the inverse power of ten. Structural quantities such as density profile, structure factor, and orientational order parameter are computed. It is shown that orientational order persists near the walls even at temperatures where the system in the bulk is in fluid state. The dependence of elastic constants, stress tensor elements, shear, and bulk moduli on density as well as the channel width is discussed. Moreover, the effect of channel incommensurability with the triangular lattice structure is discussed. It is shown that incommensurability notably affects the system properties. We compare our findings to those obtained by Monte Carlo simulations in Rici *et al.* [Phys. Rev. E **75**, 011405 (2007)] and to the case with the periodic boundary condition along the channel width.

DOI: 10.1103/PhysRevE.86.021405 PACS number(s): 82.70.Dd, 05.10.Ln, 68.55.−a, 64.60.Cn

I. INTRODUCTION

Colloidal crystals are a valuable model system, since the effective interactions between colloidal particles can be manipulated to a large extent. Furthermore, convenient techniques to observe the structure and dynamics of such systems are available [1–5]. Colloidal dispersions under geometric confinement can help us to understand the effects of confinement on the ordering of various types of nanoparticles. Related phenomena occur in a wide variety of systems, e.g., electrons at the surface of liquid helium that are confined in a quasi-one-dimensional channel [6], dusty plasmas [7], hard disks [8,9], and magnetorheological [10] colloids under confinement which are of great interest for various microfluidic and other applications. Two-dimensional (2D) colloidal dispersions have been used successfully in studies on melting in two dimensions during the last few decades [11–13]. In previous studies, much attention has been paid to the generic effect of confinement on crystalline order in $d = 2$ and to the extent and range over which the confining boundaries disturb (or enhance, respectively) the degree of order. The effect of external walls on phase behavior has been studied for a long time [14,15]. The confining wall can cause structural transition such as layering transition [16–19]. Another interesting aspect of confinement is related to formation of extended defects, solitonic staircase, and standing strain wave superstructures [20–23]. In this paper we intend to gain more insight and shed more light onto a previously studied problem, which is a 2D confined colloidal system between two walls which exert forces on the particles [24]. We implement molecular dynamics simulation and compare our findings to those obtained earlier by Monte Carlo simulations [24].

II. DESCRIPTION OF THE PROBLEM

Consider a 2D system of zero size soft disks, i.e., point particles, interacting under a purely repulsive force with the inverse power law potential $U(r) = \epsilon(\frac{\sigma}{r})^p$ where r denotes the distance between particles. The motivation for taking the spatial dimension $d = 2$ comes from experimental fact that some colloidal particles with superparamagnetic cores in the interface of water-air thin film can be described by a 2D system of particles interacting with the above repulsive potential with $p = 3$ [21,25]. However, the exponent p is taken to be 12 for computational convenience in our paper. We recall that taking $p = 3$ makes the potential long range, which is computationally inconvenient and needs special treatment. Choosing $p = 12$ has the merit that we can compare our findings with the bulk results obtained by extensive simulations [26]. We have chosen the cutoff distance $r_c = 3\sigma$ and have adopted a reduced system of units in which ϵ and σ are taken as unity ($k_B = 1$). Now we discuss how to represent the effect of confining walls. One choice is to take a smooth repulsive wall located at $x = x_{\text{wall}}$, described by a wall potential [27] $U_{\text{wall}} = \epsilon_{\text{wall}}(\frac{\sigma}{|x-x_{\text{wall}}|})^{10}$. The motivation for a decay with the 10th power is the idea that such a potential would result if we have a semi-infinite crystal with a power law interaction given by the above equation, but no cutoff, and the total potential is summed over the half space [27]. We initially set the particles on the sites of a triangular lattice which is confined between a 2D channel. The channel walls are taken to be along the y direction having a distance D from each other. The system length along the y direction is L, and periodic boundary condition is applied in the y direction. The particles number is shown by N, and the number density is given by $\rho = \frac{N}{A}$ in which $A = DL$ is the channel area. Let a_0 denotes the lattice constant in the triangular lattice (distance between nearest neighbors). The relation between ρ and a_0 is given by $\rho^{-1} = \frac{\sqrt{3}a_0^2}{2}$. Figure 1 illustrates the choice of the geometry:

*foolad@iasbs.ac.ir

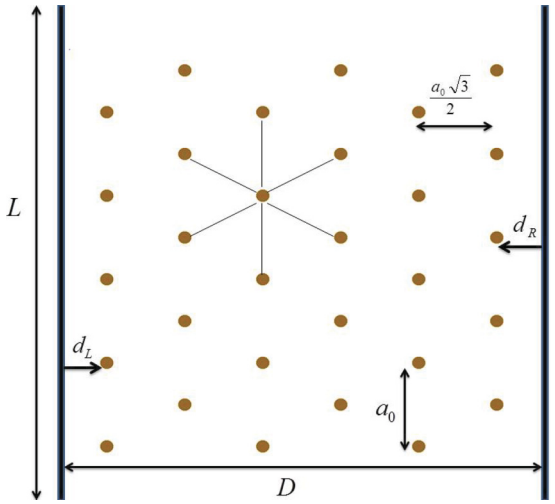

FIG. 1. (Color online) Geometry of the problem. A 2D colloidal solid with trianagular lattice structure is confined between two walls. The particles exerts repulsive forces between each other. Lattice spacing is a_0.

The left wall lies at $x = 0$, and the right wall is located at $x = D$.

We remark that one can place a triangular configuration of particles between confining walls in two different methods. In the first method, two of the six nearest neighbors of each particle are located northward and southward of it, whereas in the second method two of the six nearest neighbors are located westwards and eastwards. These two configurations are mapped into each other by a 90° rotation (see Fig. 2). As we shall see below, the elastic properties of the confined colloidal solid differs notably for these configurations. We show the distance between the first (last) column of particles from the left (right) wall by d_L (d_R), respectively. The number of columns (rows) are denoted by N_c and N_r correspondingly.

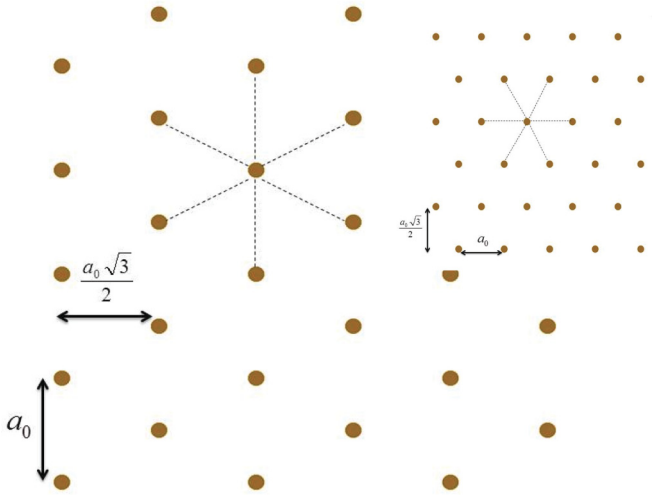

FIG. 2. (Color online) Two methods of placing particles between the confining walls. In method 1, two of the six nearest neighbors are located upwards and downwards to the central particle (main figure). In method 2 (which is rotated by 90°) two of the six nearest neighbors are located leftwards and rightwards to the central particle (upper right corner figure).

Note the number of particles is given by $N = N_c N_r$. In our simulations, we mainly have chosen $D = (N_c + 1)\frac{\sqrt{3}a_0}{2}$ with $d_L = d_R = \frac{\sqrt{3}a_0}{2}$, but we have also studied the incommensurate case where $D \neq (N_c + 1)\frac{\sqrt{3}a_0}{2}$ ($d_L \neq d_R$). In our simulations we have chosen $\epsilon_{\text{wall}} = 0.0005$ unless otherwise stated. It has been shown that by this choice, the distance between columns coincide, within error, with the ideal value $\frac{\sqrt{3}}{2}a_0$. The readers can refer to Ref. [24] for further details.

A. Simulation method and details

We have employed molecular dynamics in the *NEV* ensemble to simulate the model in the reduced units. We remark that the initial velocities are such chosen to give rise to the desired temperature when the system reaches to a steady state. The simulation parameters and details are as follows. The velocity Verlet algorithm has been used for integrating the equations of motion with a time step of $\Delta t = 0.01$, and the number of simulation time steps has been mainly chosen $T = 10^6$ where 2×10^5 time steps are discarded for equilibration. The cutoff radius $r_c = 3\sigma$ and the shifted-force potential have been taken into account.

III. STRUCTURAL PROPERTIES

In this section we present our simulation results for a narrow channel. Figure 3 shows the profile of density at two temperatures with a soft wall boundary condition with $N_c = 20$ and $N_r = 120$ for method 1 of initial triangular setting of particles. For comparison the result for a system with a periodic boundary condition (PBC) along the x direction is shown as well. The temperature $k_B T = 1$ is below the melting point for both soft walls and PBC, whereas at $k_B T = 3$ the PBC system seems to be melted but the soft wall system is not melted yet. You see in the soft wall system that the presence of confining walls enhances the density profile near the walls. A similar phenomenon is observed in the Monte Carlo simulation of the problem [24].

In Fig. 4 we compare the density profiles for methods 1 and 2 for the same temperatures as in Fig. 3. At low temperatures the results are close to each other, and there is no qualitative difference. When the temperature is raised to $k_B T = 3$ the difference between two methods becomes noticeable. Near walls the density profile is the same, but when we leave the walls and approach the center, the method 2 system melts easier than the method 1 system. This suggest that the method 1 system is more stiff and exhibits a higher persistence to melting than the method 2 system. The reason is due to the number of particles per unit length in the adjacent column to the walls. In method 1 this number is proportional to $\frac{1}{a_0}$, whereas in method 2 this number is proportional to $\frac{1}{\sqrt{3}a_0}$, which is smaller. Consequently in method 2 the force per unit length exerted by a wall to its adjacent column of particles is smaller.

In Fig. 5 the density profiles for a temperature above the melting points for both methods 1 and 2 as well as PBC are shown. Note that in the soft wall boundary condition, the system favors preserving its layering structure near the walls. In the soft wall boundary condition the profiles of methods

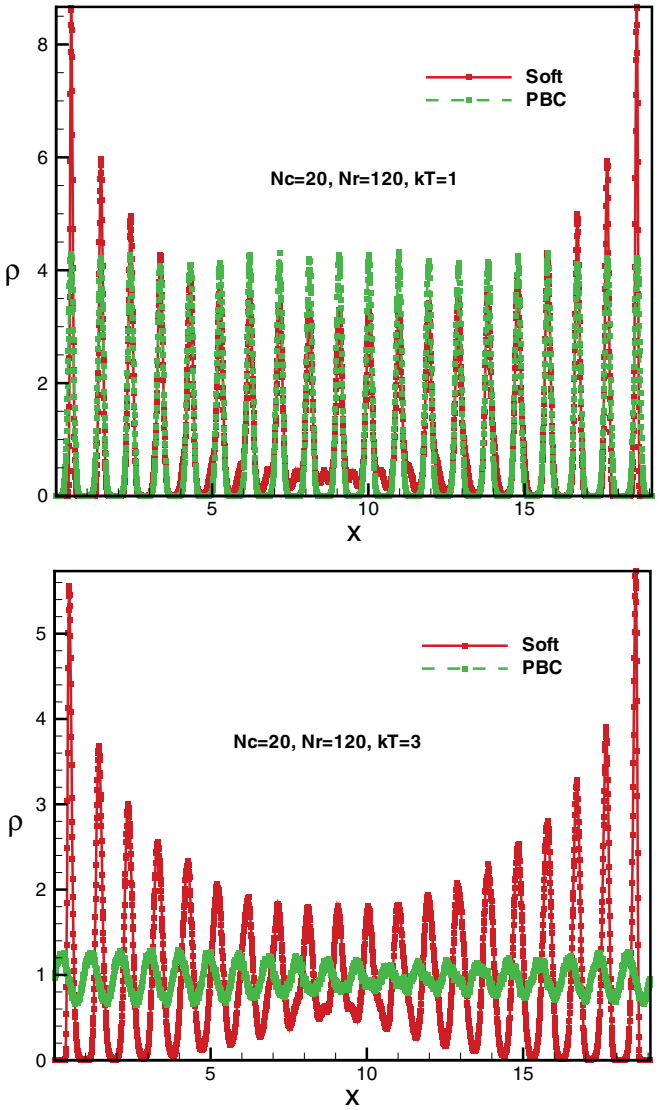

FIG. 3. (Color online) Density profile for a narrow channel with $N_c = 20$ and $N_r = 120$ at two different temperatures. Both boundary conditions, soft wall (method 1) and periodic, are sketched. Top: $k_BT = 1$, bottom: $k_BT = 3$.

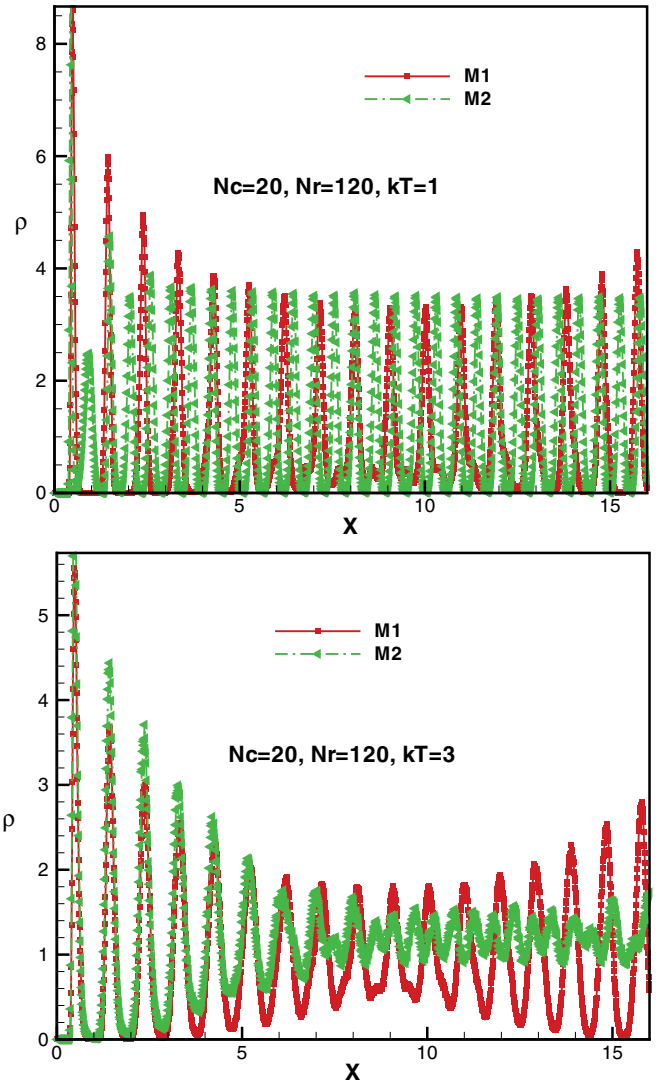

FIG. 4. (Color online) Density profile for a narrow channel with $N_c = 20$ and $N_r = 120$ at two different temperatures. The soft wall boundary condition with both methods 1 and 2 is considered. Top: $k_BT = 1$, bottom: $k_BT = 3$.

1 and 2 are almost similar to each other. As stated earlier, in method 2, the melting in the center is more evident.

Next we exhibit the structure factor $S(\mathbf{q})$ in Fig. 6 for a temperature below the melting point where the colloidal system is in the solid phase. The boundary condition is soft walls. We recall the definition of the structure factor $S(\mathbf{q})$:

$$S(\mathbf{q}) = \frac{1}{N}\sum_{l,m}\langle e^{i\mathbf{q}\cdot(\mathbf{r}_l-\mathbf{r}_m)}\rangle, \tag{1}$$

where $\langle\rangle$ denotes time averaging. We show this quantity for both methods of initial setting. Note in method 1 we have taken $\mathbf{q} = (q,0)$, whereas in method 2 we took $\mathbf{q} = (0,q)$. The sharp peaks confirms the solid structure of the system. The first (largest) peak is associated with the nearest neighbor distance a_0.

To give a quantitative description of the degree of order in the system, we obtain the orientational order parameter Ψ_6. This quantity is related to the local orientational order parameter associated with each particle k:

$$\Psi_6(k) = \frac{1}{6}\sum_{j(n.n.of\,k)} e^{6i\phi_{jk}}, \tag{2}$$

where ϕ_{jk} denotes the angle between a reference line (here the positive y axis) and the line connecting particle k to particle j. Figure 7 shows the profile of the orientational order parameter squared modulus for a narrow channel at various temperatures at $\rho = 1.05$ for the soft wall system. As you can see the modulus of Ψ_6 is greater near walls than in the channel center. Similar to the density profile, the walls enhance the degree of orientatinal order near them. The results of Monte Carlo simulations show quite similar behavior [24]. As you can see there is notable difference between methods 1 and 2 of initial triangular setting at high temperatures. Method 1 has higher orientational order than method 2, which can be attributed

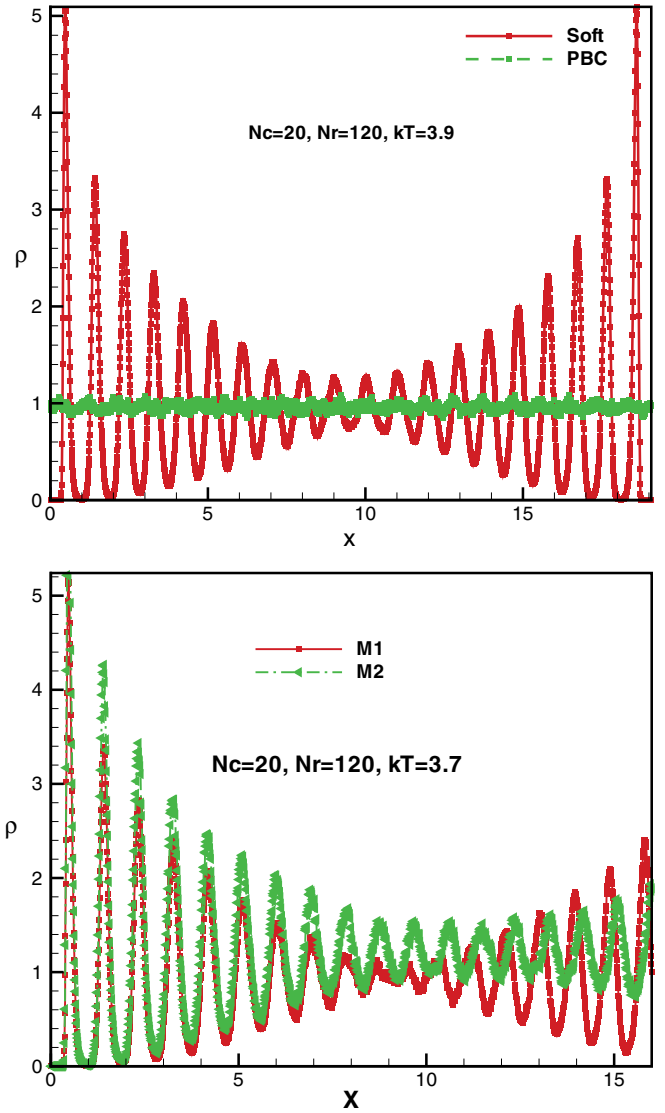

FIG. 5. (Color online) Top: Density profile for a narrow channel with $N_c = 20$ and $N_r = 120$ at a temperature above the melting point for both boundary conditions, soft wall and periodic. Bottom: Comparison of methods 1 and 2 in the soft wall boundary condition.

to its higher stiffness. The difference gets sharper when the temperature arises.

Figure 8 shows the dependence of the orientational order parameter squared modulus at the channel center as well as near its walls versus T at $\rho = 1.05$ for both methods 1 and 2. These results are in qualitative agreement with MC results [24]. When the vicinity of the walls are considered, only a monotonous decrease with the temperature is observed. On the other hand, when the channel center is considered, a change in the slope emerges which can be attributed to system melting in the center. By increasing the temperature, the difference between methods 1 and 2 becomes enhanced.

IV. ELASTIC CONSTANTS

Apart from the study of the lattice structure, positional and orientational order parameters, and structural properties, there

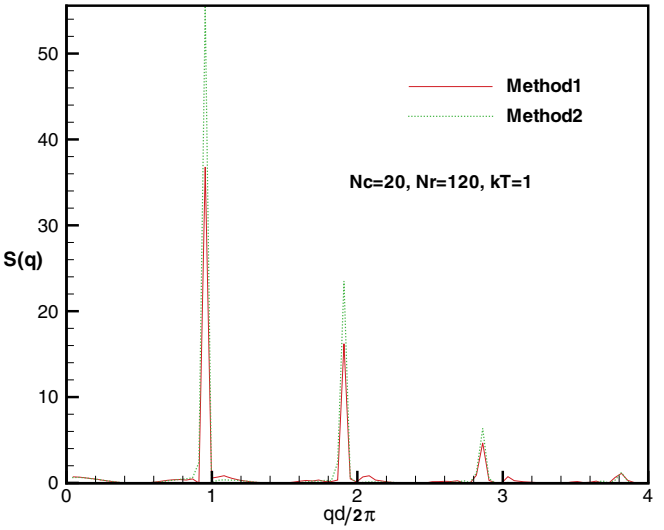

FIG. 6. (Color online) Structure factor $S(q)$ for a narrow channel with the soft wall boundary condition at a temperature $k_BT = 1$ for initial setting. Methods 1 and 2 give identical results.

is also considerable interest in the mechanical properties and in particular elastic constants of 2D crystals. The dependence of these elastic constants on temperature (or density, respectively) plays a crucial role in the theory of 2D melting [13,28,29]. One expects a significant effect of the symmetry of the crystal structure. The Voigt notation has been implemented here [30]. In two dimensions we have four elastic constants, $C_{11}, C_{22}, C_{12}, C_{33}$. In this paper we have implemented the method of stress fluctuation to obtain the elastic constants [31,32]. This method which is based on an atomic-level description was originally introduced by Born and Huang [33]. The contribution from the particles to the elastic constants are

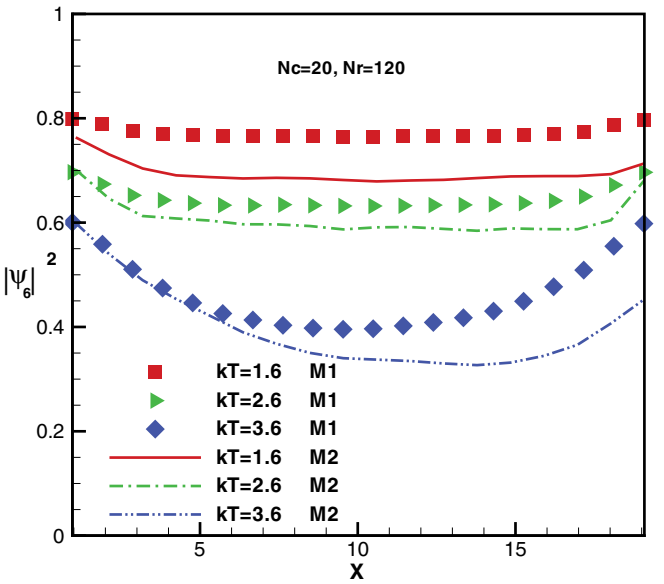

FIG. 7. (Color online) The squared modulus of the orientational order parameter profile Ψ_6 of a narrow channel with the soft-wall boundary condition at $\rho = 1.05$ for various temperature values. Methods 1 and 2 are shown.

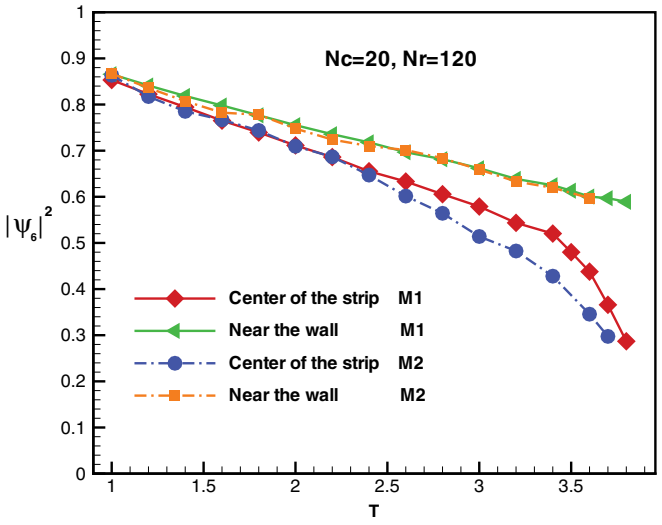

FIG. 8. (Color online) Temperature dependence of the orientational order parameter squared modulus at the center as well as near the channel walls. Methods 1 and 2 are compared to each other.

as follows:

$$C_{\alpha\beta\gamma\delta}(i) = \frac{1}{2\Omega(i)} \sum_{j\neq i} \left(\frac{\phi''(r_{ij})}{r_{ij}^2} - \frac{\phi'(r_{ij})}{r_{ij}^3} \right) [x_\alpha(j) - x_\alpha(i)] \times [x_\beta(j) - x_\beta(i)][x_\gamma(j) - x_\gamma(i)][x_\delta(j) - x_\delta(i)] + \frac{\phi'(r_{ij})}{r_{ij}} [x_\beta(j) - x_\beta(i)][x_\gamma(j) - x_\gamma(i)]\delta_{\alpha\delta}. \quad (3)$$

Note that the term proportional to $\delta_{\alpha\delta}$ should not be considered in the soft wall case. The contribution from a wall is obtained from the following relation:

$$C_{\alpha\beta\gamma\delta}(i) = \frac{1}{2\Omega(i)} \left[\frac{1}{x_i^2} \phi_W''(x_i) - \frac{1}{x_i^3} \phi_W'(x_i) \right] \left[x_\alpha^W - x_\alpha(i) \right] \times \left[x_\beta^W - x_\beta(i) \right] \left[x_\gamma^W - x_\gamma(i) \right] \left[x_\lambda^W - x_\lambda(i) \right], \quad (4)$$

in which ϕ_W is the wall potential imposed on the particles. Also note that $x_y^W = y_i$ and $x_x^W = 0$ for the left wall and $x_x^W = D$ for the right wall. Figure 9 shows the dependence of elastic constants in a narrow channel versus the density in the solid phase. The soft wall boundary condition is implemented, and both methods of initial triangular setting are considered. All the components increase with increment of ρ. This seems natural since the solid becomes more tough when the density is increased. Except for C_{11} for which both methods give identical results, the other three components of the elastic tensor show notable difference for methods 1 and 2. For C_{12}

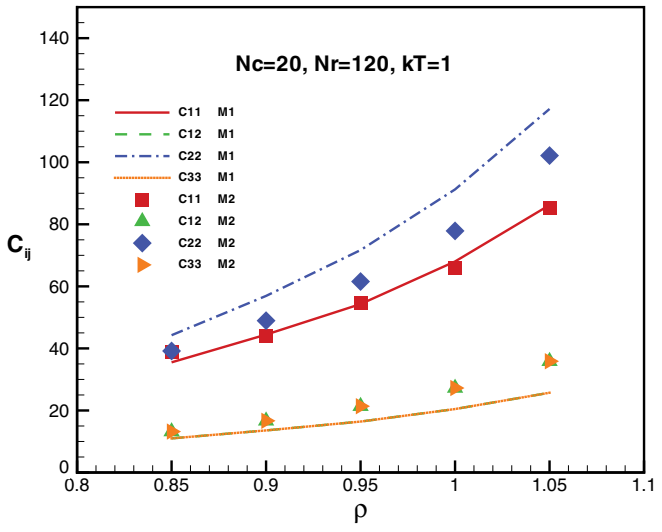

FIG. 9. (Color online) Dependence of the elasticity tensor components on density in the soft wall boundary condition at $k_BT = 1$ for both methods 1 and 2. The values of the elastic constants show a substantial difference in methods 1 and 2.

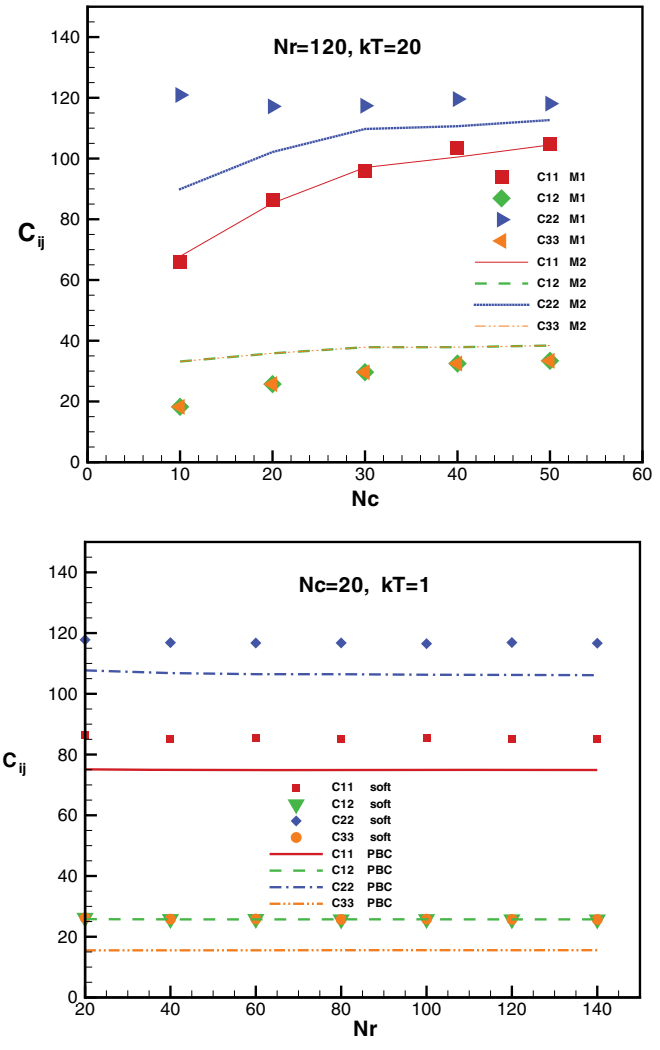

FIG. 10. (Color online) Top: Dependence of the elasticity tensor components on the number of columns N_c for the soft wall system at $k_BT = 1$ for both methods 1 and 2. Bottom: Dependence of the elastic tensor components on the number of rows N_r for both the soft wall (method 1) and periodic boundary conditions at $k_BT = 1$. The value for the elasticity tensor components in the PBC are smaller than the corresponding values in the soft wall boundary condition.

and C_{33} method 2 has a higher value in a given density, whereas for C_{22} the method 1 value is larger than method 2.

In order to have a further insight into the problem, we have investigated the dependence of elastic constants at a give density ($\rho = 1.05$) on the channel width D. Figure 10 exhibits the dependence of elastic constants on the number of columns N_c and the rows N_r.

The channel width $D = (N_c + 1)\frac{\sqrt{3}a_0}{2}$ plays a noticeable role. The constant C_{11} is mostly affected by the channel width. C_{22} is least affected. After N_c increases beyond 60 (which equals to $\frac{N_r}{2}$) the channel width D plays almost no role and the values approach the bulk ones. Our results in Fig. 10(a) are in qualitative agreement with those by Monte Carlo simulations [24]. The main difference is that in our results C_{12} and C_{33} coincide with each other when the system width becomes large, whereas in Ref. [24] they do not. Notice that the symmetry $C_{12} = C_{33}$ is expected in the bulk. The values of our elastic constants are less than those in Ref. [24]. We remark that the channel length in Ref. [24] ($N_r = 30$) is not the same as ours ($N_r = 120$). Similar to the previous graph, for C_{11} methods 1 and 2 give almost identical results. Also for a given width D, C_{12} and C_{33} are larger for method 2 while C_{22} is smaller. Molecular dynamics simulation allows us to compute the components of the stress tensor by averaging over the system particles trajectories. The stress tensor elements can, in principle, be evaluated from the particles trajectories. There are two contributions: one from the particles and the other from the walls. The contribution from the particles to the stress tensor component associated to particle i turns out to be [32]

$$\sigma_{\alpha\beta}(i) = \frac{1}{2\Omega(i)} \sum_{j \neq i} \frac{1}{r_{ij}} \phi'(r_{ij})[x_\alpha(j) - x_\alpha(i)][x_\beta(j) - x_\beta(i)]. \tag{5}$$

To evaluate the wall contribution, we assume each wall as a fixed particle with infinite mass at the same height of particle i. With this in mind, the contribution of the left wall which is located at $x_{\mathrm{LW}} = 0$ becomes

$$\sigma^{\mathrm{LW}}_{\alpha\beta}(i) = \frac{1}{2\Omega(i)} \phi'_{\mathrm{LW}}(x_i)\delta_{\alpha,x} x_\beta(i), \tag{6}$$

in which $\phi_{\mathrm{LW}}(x_i)$ is the potential energy between the left wall and particle i. Similarly, the contribution from the right wall yields

$$\sigma^{\mathrm{RW}}_{\alpha\beta}(i) = \frac{1}{2\Omega(i)} \phi'_{\mathrm{RW}}(D - x_i)\delta_{\alpha,x}[D - x_\beta(i)]. \tag{7}$$

Dependence of the stress tensor components on the density for a temperature below melting is shown in Fig. 11.

As can be seen, the symmetry $\sigma_{xy} = \sigma_{yx}$ is fulfilled. There is a notable dependence for the nonzero components σ_{xx} and σ_{yy} on the density. By increasing the density ρ, they tend to decrease. As you can see there is not much difference between methods 1 and 2. In Fig. 12 we have sketched the dependence of bulk and shear moduli B and μ on ρ and N_c for a narrow channel with the soft wall boundary condition for methods 1 and 2. These quantities increase nonlinearly with the density

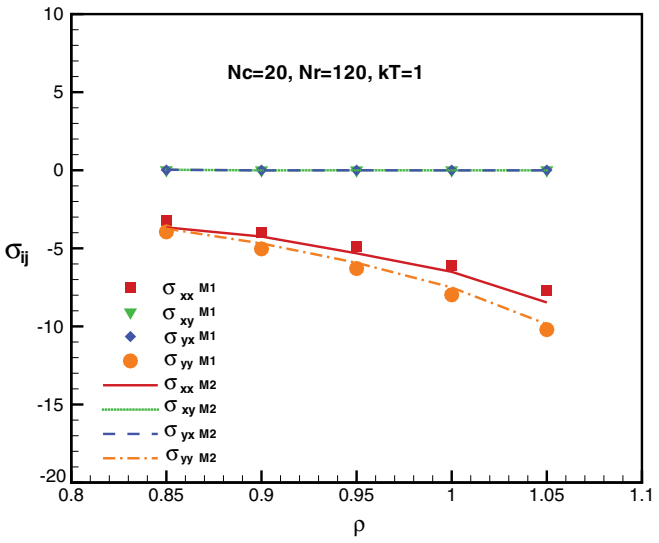

FIG. 11. (Color online) Dependence of the stress tensor components on the density for a narrow channel with the soft wall boundary condition in the solid phase (methods 1 and 2 are exhibited).

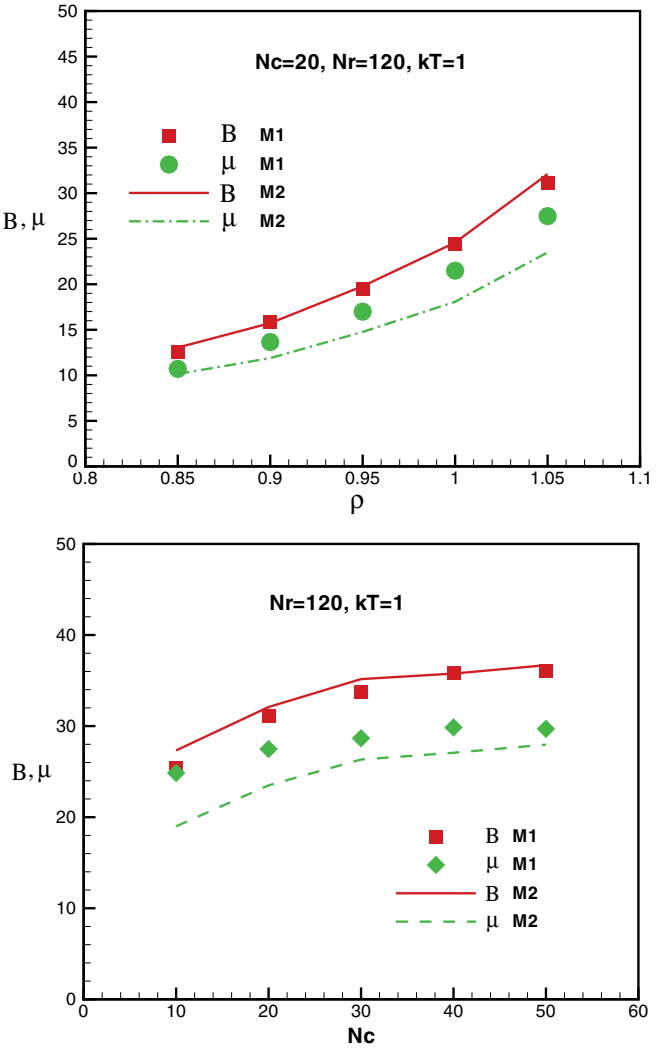

FIG. 12. (Color online) Top: Density dependence of the bulk and shear mudulii B and μ in the solid phase soft wall boundary condition. Bottom: Column number dependence of the bulk and shear moduli B and μ in the solid phase. Methods 1 and 2 are compared.

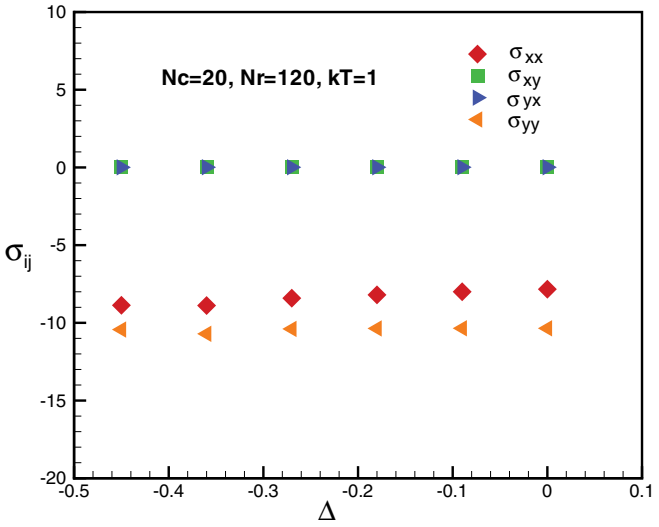

FIG. 13. (Color online) Dependence of the stress tensor components on the incommensurability parameter Δ. The results are for method 1 of the soft wall boundary condition.

ρ. Again we see that beyond $N_c = \frac{N_r}{2}$ there is almost no dependence on N_c. In comparison between methods 1 and 2, we see that the bulk modulus does not show significant change but the shear modulus does. In fact, method 2 gives a larger shear modulus which is expected since the method 2 system has a smaller degree of stiffness and hence larger shear modulus.

V. CHANNEL WITH INCOMMENSURATE WIDTH TO TRIANGULAR LATTICE

In the previous sections, the channel width D was carefully chosen such that the ideal triangular lattice structure fits into the channel as perfectly as possible. It would be interesting to see what happens when such a choice is not made, and D does not correspond to an integer multiple of the distance between columns $d = \frac{\sqrt{3}a_0}{2}$ (method 1). Such questions have

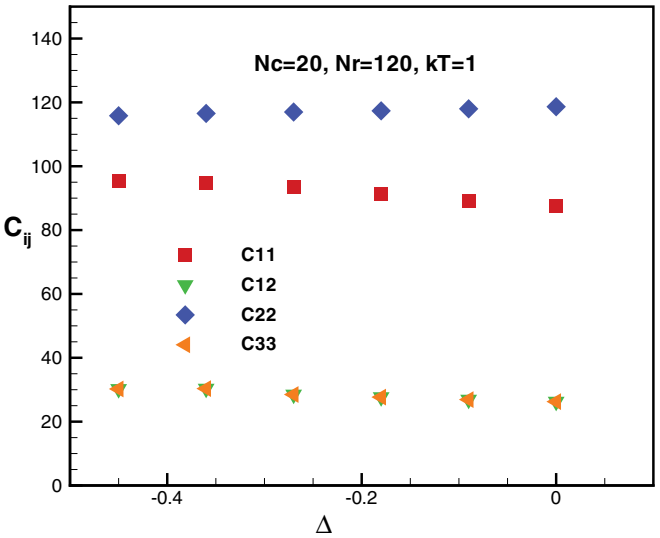

FIG. 14. (Color online) Dependence of the elasticity tensor components on the incommensurability parameter Δ for method 1.

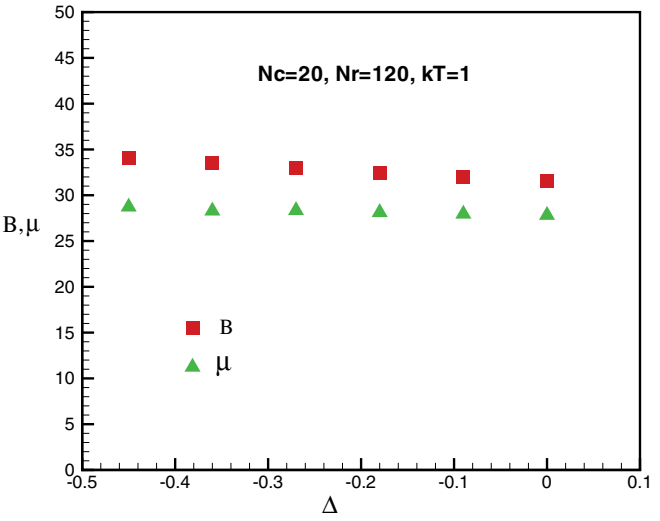

FIG. 15. (Color online) Dependence of B and μ on the incommensurability parameter Δ for method 1.

been considered in the literature (e.g., Refs. [24]) for ultrathin strips, and structures rather rich in defects were found. Here we investigate the impact of the incommensurability on the system characteristics. Figures 13 and 14 show the dependence of stress and elasticity tensor components on the incommensurability parameter Δ, which is defined as $d_R = \frac{\sqrt{3}a_0}{2} + \Delta$. We observe the bulk and shear moduli are mostly affected by variations of Δ, whereas stress and elasticity components are less affected. In Fig. 13 we see that σ_{xy} and σ_{yx} do not show any significant dependence on Δ, whereas the diagonal elements σ_{xx} and σ_{yy} exhibit quite noticeable dependence on Δ. In Fig. 14 we observe that in the incommensurate system the elasticity tensor components decrease when Δ in increased.

Eventually in Fig. 15 we have shown the dependence of bulk and shear moduli on Δ. Similar to elasticity tensor, by increasing the degree of incommensurability the bulk and shear moduli decrease. The amount of decrease is quite sharp.

VI. SUMMARY AND CONCLUSION

We have used molecular dynamics simulations to study the effect of confinement on a 2D crystalline solid, with triangular structure, of point particles interacting with an inverse power law potential proportional to r^{-12} in a narrow channel. Two methods of initial setting of particles in a triangular lattice are discussed. The system characteristics depend sensitively on the interaction of the two *walls* providing the confinement. The walls exert perpendicular forces on their adjacent particles. Some structural quantities, namely, density profile, structure factor, and orientational order parameter are computed, and their dependence on temperature, density, and other system parameters are evaluated. It is shown that orientational order persists near the walls even at temperatures where the system in the bulk is in the fluid state. Moreover, the dependence of elastic constants, stress tensor elements, shear and bulk moduli on density as well as the channel width is discussed, and it is shown that they increase with raising the density. The effect of varying the channel width is explored, and it is found that in general the bulk and shear moduli increase

with increasing the channel width until the width becomes comparable to the system length. Furthermore, the effect of incommensurability of the channel with the triangular lattice structure is discussed. It is shown that incommensurability notably affects the system properties. We compare our findings to those obtained by Monte Carlo simulations in Ref. [24] and to the periodic boundary condition along the channel.

ACKNOWLEDGMENTS

We are highly indebted to Prof. Surajit Sengupta for his valuable comments and fruitful discussions. We wish to express our gratitude to Prof. Hashem Rafii Tabar and Dr. Abbas Montazeri for their useful help and enlightening discussions. M.E.F is thankful to No'rooz Khan for his valuable discussions.

[1] W. C. Poon and P. N. Pusey, in *Observation, Prediction and Simulation of Phase Transitions in Complex Fluids*, edited by M. Baus, F. Rull, and J. P. Ryckaert (Kluwer, Dordrecht, 1995), p. 3.
[2] H. Löwen, J. Phys.: Condens. Matter **13**, 415R (2001).
[3] *Coloidal Dispersions in External Fields*, edited by H. Löwen and C. N. Likos, special issue of J. Phys.: Condens. Matter **16**(38), S4231 (2004).
[4] P. N. Pusey, in *Liquids, Freezing and the Glass Transition*, edited by J. P. Hansen, D. Levesque, and J. Zinn-Justin (North Holland, Amsterdam, 1991).
[5] K. Zahn, A. Wille, G. Maret, S. Sengupta, and P. Nielaba, Phys. Rev. Lett. **90**, 155506 (2003).
[6] P. Glasson, V. Dotsenko, P. Fozooni, M. J. Lea, W. Bailey, G. Papageorgiou, S. E. Andresen, and A. Kristensen, Phys. Rev. Lett. **87**, 176802 (2001).
[7] Y.-L. Lai and I. Lin, Phys. Rev. E **64**, 015601(R) (2001).
[8] P. Pieranski *et al.*, Mol. Phys. **40**, 225 (1980).
[9] D. Chaudhuri and S. Sengupta, Phys. Rev. Lett. **93**, 115702 (2004).
[10] R. Haghgooie and P. S. Doyle, Phys. Rev. E **70**, 061408 (2004).
[11] K. J. Strandburg, Rev. Mod. Phys. **60**, 161 (1988); **61**, 747 (1989).
[12] S. Sengupta, P. Nielaba, and K. Binder, Phys. Rev. E **61**, 6294 (2000).
[13] K. Binder, S. Sengupta, and P. Nielaba, J. Phys.: Condens. Matter **14**, 2323 (2002).
[14] K. Binder and P. C. Hohenberg, Phys. Rev. B **6**, 3461 (1972); **9**, 2194 (1974).
[15] K. Binder, in *Phase Transitions and Critical Phenomena*, edited by C. Domb and J. L. Lebowitz, Vol. 8 (Academic, London, 1983), p. 1.
[16] P. G. de Gennes, Langmuir **6**, 1448 (1990).
[17] J. Gao, W. D. Luedtke, and U. Landman, Phys. Rev. Lett. **79**, 705 (1997).
[18] A. Chaudhuri, S. Sengupta, and M. Rao, Phys. Rev. Lett. **95**, 266103 (2005).
[19] D. Chaudhuri and S. Sengupta, J. Chem. Phys. **128**, 194702 (2008).
[20] A. Blaaderen, Prog. Colloid Polym. Sci. **104**, 59 (1997).
[21] K. Zahn and G. Maret, Phys. Rev. Lett. **85**, 3656 (2000).
[22] G. Piacente, I. V. Schweigert, J. J. Betouras, and F. M. Peeters, Phys. Rev. B **69**, 045324 (2004).
[23] Y. H. Chui and S. Sengupta, I. K. Snook, and K. Binder, J. Chem. Phys **132**, 074701 (2010).
[24] A. Ricci, P. Nielaba, S. Sengupta, and K. Binder, Phys. Rev. E **75**, 011405 (2007).
[25] K. Zahn, J. M. Mendez-Alcaraz, and G. Maret, Phys. Rev. Lett. **79**, 175 (1997).
[26] K. Bagchi, H. C. Andersen, and W. Swope, Phys. Rev. E **53**, 3794 (1996).
[27] P. Nielaba, K. Binder, D. Chaudhuri, K. Franzrahe, P. Henseler, M. Lohrer, A. Ricci, S. Sengupta, and W. Strepp, J. Phys.: Condens. Matter **16**, S4115 (2004).
[28] B. I. Halperin and D. R. Nelson, Phys. Rev. Lett. **41**, 121 (1978).
[29] A. P. Young, Phys. Rev. B **19**, 1855 (1979).
[30] P. M. Chaikin and T. C. Lubensky, *Principles of Condensed Matter Physics* (Cambridge University Press, Cambridge, England, 1995).
[31] K. Nishioka, T. Takai, and K. Hata, Philos. Mag. A **65**, 227 (1992).
[32] H. Rafii-Tabar, Phys. Rep. **390**, 235 (2004).
[33] M. Born and K. Huang, *Dynamical Theory of Crystal Lattices* (Clarendon Press, Oxford, 1954).